The root-knot nematode effector MiPDI1 targets a stress-associated protein (SAP) to establish disease in Solanaceae and Arabidopsis

Jianlong Zhao, Joffrey Mejias, Michaël Quentin, Yongpan Chen, Janice Almeida-engler, Zhenchuan Mao, Qinghua Sun, Qian Liu, Bingyan Xie, Pierre Abad, et al.

The root-knot nematode effector MiPDI1 targets a stress-associated protein, SAP, to establish disease in Solanaceae and *Arabidopsis*

Jianlong Zhao[1,2,3], Joffrey Mejias[3], Michael Quentin[3], Yongpan Chen[1,3], Janice de Almeida-Engler[3], Zhenchuan Mao[2], Qinghua Sun[2], Qian Liu[1], Bingyan Xie[2], Pierre Abad[3], Bruno Favery[3*] and Heng Jian[1*]

*** co-corresponding authors**

[1]Department of Plant Pathology and Key Laboratory of Pest Monitoring and Green Management of the Ministry of Agriculture, China Agricultural University, Beijing, China

[2]Institute of Vegetables and Flowers, Chinese Academy of Agricultural Science, Beijing, China

[3]INRAE, Université Côte d'Azur, CNRS, ISA, F-06903 Sophia Antipolis, France

*** Author for correspondence**

Pr. Heng Jian

Yuanmingyuan West Road No. 2, Haidian District, Beijing, China

Tel: +86 135 5248 1996

Email: hengjian@cau.edu.cn

Dr. Bruno Favery

400 route des chappes, BP 167, 0690 Sophia Antipolis, France

Email: bruno.favery@inrae.fr

Jianlong Zhao zhaojianlong@caas.cn,

Joffrey Mejias joffrey.mejias@etu.univ-cotedazur.fr,

Michael Quentin michael.quentin@inrae.fr,

Yongpan Chen chenyongpan1@163.com,

Janice de Almeida-Engler janice.de-almeida@inrae.fr,

Zhenchuan Mao maozhenchuan@caas.cn,

Qinghua Sun sunqinghua_h@163.com,

Qian Liu liuqian@cau.edu.cn,

Bingyan Xie xiebingyan@caas.cn,

Pierre Abad pierre.abad@inrae.fr,

Bruno Favery bruno.favery@inrae.fr,

Heng Jian hengjian@cau.edu.cn

Total word count

5,651 words (Introduction, 851; Materials and Methods, 1,830; Results, 1,416; Discussion, 1,402; Acknowledgements, 151).

Figures: 6 (All figures in colour).

Supporting information files: 11 (3 tables and 8 figures).

Summary

- Large amounts of effectors are secreted by the oesophageal glands of plant-parasitic nematodes, but their molecular mode of action remains largely unknown. We characterised a *Meloidogyne incognita* protein disulphide isomerase (PDI)-like effector protein (MiPDI1) that facilitates nematode parasitism.
- *In situ* hybridisation showed that *MiPDI1* was expressed specifically in the subventral glands of *M. incognita*. It was significantly upregulated during parasitic stages. Immunolocalisation demonstrated MiPDI1 secretion *in planta* during nematode migration and within the feeding cells. Host-induced silencing of the *MiPDI1* gene affected the ability of the nematode to infect the host, whereas *MiPDI1* expression in *Arabidopsis* increased susceptibility to *M. incognita*, providing evidence for a key role of MiPDI1 in *M. incognita* parasitism.
- Yeast two-hybrid assays, BiFC and Co-IP showed that MiPDI1 interacted with a tomato stress-associated protein (SlSAP12) orthologous to the redox-regulated AtSAP12, which plays an important role in plant responses to abiotic and biotic stresses. *SAP12* silencing or knocking out in *N. benthamiana* and Arabidopsis increased susceptibility to *M. incognita.*
- Our results suggest that MiPDI1 acts as a pathogenicity factor promoting disease by fine-tuning SAP-mediated responses at the interface of redox signalling, defence and stress acclimation in Solanaceae and *Arabidopsis*.

Key words: plant-parasitic nematodes, effector, stress, redox, giant cells

Introduction

Plant parasitic nematodes are among the most economically devastating plant pathogens, causing global yield losses of more than 100 billion dollars each year (Abad *et al.*, 2008). The obligate sedentary endoparasitic nematodes causing the most severe problems are root-knot nematodes (RKNs) and cyst nematodes (CNs). The RKNs, *Meloidogyne* spp., can infest more than 5,500 crop species (Blok *et al.*, 2008), and therefore represent a huge threat to agricultural production. After hatching, the infective second-stage juveniles (J2s) are attracted to the tip of plant roots. They penetrate the root elongation zone and migrate between cells to reach the vascular cylinder of the plant. There, they become sedentary, and construct a feeding site. This feeding site consists of around seven multinucleate giant cells, resulting from nuclear divisions and isotropic growth, surrounded by cells that divide and initiate vascular differentiation. The giant cells are the sole source of nutrients for the developing nematode (Favery *et al.*, 2016). RKNs ensure that parasitism is successful by secreting a large number of effectors that help juveniles to invade roots, suppress plant defence mechanisms, and induce and maintain giant cells. These effectors are mostly produced in the three oesophageal glands, but they may also be secreted by other organs, such as the amphids and hypodermis (Mejias *et al.*, 2019; Vieira & Gleason, 2019). The precise localisation of effectors and the identification of their host targets are essential for a better understanding of their biological functions. Only a few host target proteins of RKN effectors have been identified to date (Mejias *et al.*, 2019). The *M. incognita* effector Mi16D10 has been shown to interact with *Arabidopsis* SCARECROW-like transcription factors (Huang *et al.*, 2006). The *M. graminicola* effector MgMO237 has been shown to interact with three rice defense-related proteins (OsGSC, OsCRRSP55 and OsBetvI) (Chen *et al.*, 2018) and the Mg16820 and *M. chitwoodi* Mc01194 effectors interact with rice dehydration-stress inducible protein 1 (OsDIP1) and *Arabidopsis* papain-like cysteine protease (RD21A), respectively (Davies *et al.*, 2015; Naalden *et al.*, 2018). A MACROPHAGE MIGRATION INHIBITORY FACTOR-like effector, MiMIF-2, was recently shown to interact with two *Arabidopsis* annexins, mediating plant immune responses (Zhao *et al.*, 2019). However, the functions of a large number of RKN effectors, their plant targets and working mechanisms remain unknown and in need of clarification.

Protein disulphide isomerase (PDI) is a protein thiol oxidoreductase located in the eukaryotic endoplasmic reticulum. PDI has both protein disulphide isomerase and protein-glutamine gamma-glutamyltransferase activities. It is involved in the oxidoreduction and isomerisation of protein disulphide bonds, peptidyl-proline hydroxylation to 4-hydroxy-L-proline, and protein deglutathionylation (Ali Khan & Mutus, 2014). More than 50 PDI-like proteins have been identified in fungi, plants, animals and humans. The free-living nematode *Caenorhabditis elegans* has three conserved *PDI*-like genes, *PDI-1*, *PDI-2*, and *PDI-3*, and *PDI-2* has been shown to be expressed in the hypodermis and cuticle collagen (Winter & Page, 2000). Many animal parasites, including protozoans in particular, have PDI-like proteins that play major roles in parasitism (Achour *et al.*, 2002; Han *et al.*, 2014). Three PDI-like proteins in the tick *Haemaphysalis longicornis* have been shown to be expressed predominantly in the salivary glands, and blood feeding significantly increases the expression of *HlPDI-1* and *HlPDI-3* (Liao *et al.*, 2007). There are also many PDI-like proteins in malaria parasites. *Plasmodium falciparum* PfPDI-8 has specific enzyme activity and facilitates the disulphide-dependent conformational folding of a malaria protein (Mahajan *et al.*, 2006).

Secreted PDIs have also recently been characterised in plant pathogens. The PDI1 protein of *Phytophthora parasitica* (PpPDI1) is associated with haustoria-like structures and contributes to plant infection (Meng *et al.*, 2015). Two PDI-like effectors have been identified in RKNs and CNs, shown to be expressed in oesophageal glands and upregulated in late parasitic J2s or J3. A functional analysis of *Heterodera schachtii* HsPDI showed that this protein promoted parasitism by regulating the plant ROS burst (Habash *et al.*, 2017). Recombinant *M. graminicola* MgPDI protein had oxidase and isomerase activities. The expression of both *MgPDI* and *HsPDI* was induced by exogenous H_2O_2, suggesting that PDI may protect nematodes from oxidative stress (Tian *et al.*, 2019). Interestingly, PDI-like proteins were identified in the secretome of *M. incognita* juveniles (Bellafiore *et al.*, 2008) and the proteome of oesophageal gland cells from *M. incognita* females (Wang *et al.*, 2012), demonstrating that these proteins are secreted by *M. incognita*. However, the detailed mode of action and plant targets of PDI-like effectors remain unknown.

In this study, we characterised a new *PDI-like* gene from *M. incognita* cDNA (*MiPDI1*) that is expressed in the subventral oesophageal glands. Immunohistochemical staining of tomato root sections with an anti-MiPDI1 antibody showed that this protein was secreted into infected roots. Our findings also showed that MiPDI1 was important for nematode infection. Yeast two-hybrid assays, BiFC and Co-IP showed that MiPDI1 interacted physically with a stress-associated protein (SlSAP12) from tomato. Virus-induced gene silencing (VIGS) of orthologues in knockout lines of *N. benthamiana* and *Arabidopsis* resulted in higher levels of *M. incognita* infection. Moreover, MiPDI1 expression *in planta* affects the expression of *Arabidopsis* defence-associated genes. Our data suggest that MiPDI1 may act as a novel effector, promoting *M. incognita* parasitism by fine-tuning SAP-mediated host responses.

Materials and methods

Nematodes and plant materials

Egg masses of *M. incognita* (Morelos strain) were collected from tomato plants (*Solanum lycopersicum* cv St Pierre). The hatched preparasitic second-stage juveniles (pre-J2s) were collected for plant inoculation. Various *M. incognita* stages were isolated from digested tomato roots, as previously described (Zhao *et al.*, 2019). Surface-sterilised *Arabidopsis thaliana* seeds (ecotype Col-0) were sown on Murashige and Skoog (MS) medium in sterile conditions. After germination, the plantlets were transplanted into pots containing soil and sand (1:1) and grown at 21°C. The T-DNA mutant line for *AtSAP12* (*At3g28210*) (*SALK_014706*) was obtained from the *Arabidopsis* Biological Resource Center (ABRC, USA). *Nicotiana benthamiana*, *Solanum lycopersicum* and *N. tabacum* plants were grown at 24°C (photoperiod, 16 h : 8 h, light : dark).

Sequence analysis, alignment and phylogenetic tree

MiPDI sequences were obtained from *Meloidogyne* genomic resources (http://www6.inra.fr/meloidogyne_incognita/). Sequences were aligned with the MAFFT tool on the EBI server (https://www.ebi.ac.uk/Tools/msa/mafft/). The alignment obtained was used as input for the IQTree Web server (http://iqtree.cibiv.univie.ac.at/) (Trifinopoulos *et al.*, 2016),

to generate the maximum likelihood phylogenetic tree. The model chosen by the inbuilt model test was LG+F+I+G4. Support for the nodes was calculated with a hundred bootstrap replicates. PpPDI was used as the outgroup. The tree was visualised in iTOL (https://itol.embl.de/).

RNA extraction and real-time quantitative RT-qPCR

A Dynabeads® mRNA DIRECT™ kit (Invitrogen, USA) was used to extract mRNA from *M. incognita*. Arabidopsis, tomato and tobacco total RNA were extracted with TRIzol Reagent (Invitrogen, USA). We synthesised cDNA with the reverse transcriptase SuperScript III (Invitrogen, USA), in accordance with the manufacturer's instructions. RT-qPCR was performed with an ABI Prism 7000 (Applied Biosystems, USA) real-time PCR system (the primers are shown in Table S1). *M. incognita GAPDH* (*Minc12412*) and *HK14* (*Minc18753*) or *A. thaliana OXA1* (AT5G62050) and *UBP22* (AT5G10790) were used as internal controls for the normalisation of RT-qPCR data. PCR was performed with SYBR Premix Ex Taq (TaKaRa, Japan), as follows: 95°C for 30 s, followed by 40 cycles of 95°C for 5 s, 60°C for 31 s, and 95°C for 15 s, 60°C for 60 s, and 95°C for 15 s. Data were analysed by the $2^{-\Delta\Delta Ct}$ method (Livak & Schmittgen, 2001). Three technical replicates for two to four independent biological experiments were performed.

***In situ* hybridisation (ISH) of *MiPDI1* and immunolocalisation in preparasitic J2s**

ISH was performed on freshly hatched *M. incognita* preparasitic J2s (pre-J2s), as previously described (Jaouannet *et al.*, 2018). The *MiPDI1* was amplified with the specific primers ISH-PDI-F and –R (Table S1). Immunolocalisation was performed as previously described (Jaubert *et al.*, 2002; Jaubert *et al.*, 2005). A polyclonal antibody against MiPDI1 was produced with a specific peptide (KEGSPPSENSLDDLVE). Western blotting was performed to check the specificity of this antibody. Immunolocalisation was performed directly on *M. incognita* pre-parasitic J2s with the anti-MiPDI1 antibody (1:300) and the Alexa Fluor 488-conjugated goat anti-rabbit antibody (1:500) (Molecular Probes, Eugene). As a negative control, nematodes were incubated with pre-immune serum. Images were collected with a confocal microscope

(Zeiss LSM880, Germany).

Immunohistochemistry on tomato gall sections

Tomato galls were collected 5 and 10 days post infection (dpi) with *M. incognita,* cut into small pieces with a razor blade in a Petri dish and fixed in 8% formaldehyde in 50 mM piperazine-N, N'-bis (ethanesulphonic acid) (PIPES) buffer (pH 6.9). The immunolocalisation procedure was performed essentially as previously described (de Almeida Engler *et al.*, 2004). Galls were dehydrated and embedded in butyl-methylmethacrylate and sections were incubated in acetone for 30 min to remove the butyl-methylmethacrylate. Slides containing 5 µm-sectioned galls were then treated with a series of ethanol solutions and incubated in a blocking solution of 1% BSA. Sections were subsequently incubated with anti-MiPDI1 antibody (1:300) at 4 °C overnight and then at 37 °C for 2 hours in a damp box. As a negative control, gall sections were incubated with pre-immune serum. Finally, slides were incubated with Alexa Fluor 488-conjugated goat anti-rabbit antibody (Molecular Probes, Eugene) and cell nuclei were stained with 4', 6-diamidino-2-phenylindole (DAPI) (Sigma, USA). Images were captured at an excitation wavelength of 488 nm by confocal microscopy (Zeiss LSM880, Germany).

***In planta* RNAi, DEX-induced *MiPDI1* expressing Arabidopsis lines and RKN infection assay**

MiPDI1 fragments (forward and reverse) were amplified with primers (Table S1) inserted separately into the forward and backward sequences of the pSAT5 intron of the pSuper-RNAi vector (Dafny-Yelin *et al.*, 2007). The *MiPDI1* coding sequence (cds) without the signal peptide sequence for secretion (MiPDI1 woSP) was amplified (Table S1) and inserted into the PTA7001 vector (a gift from Professor Wenxian Sun, China Agricultural University) to generate PTA7001-MiPDI1-FLAG. These vectors were used to transform *Agrobacterium tumefaciens* GV3101, which was in turn used to transform *A. thaliana* Col-0 (WT) by the floral dip method (Zhang *et al.*, 2006). Homozygous T3 plants from three pdi-Ri lines and two MiPDI-FLAG lines were used. Lines were verified by western blotting after induction with 30

μM dexamethasone (DEX). The homozygous gfp-Ri T3 lines have been described elsewhere (Zhao *et al.*, 2019). *Arabidopsis* plants were inoculated with 300 pre-J2s of *M. incognita*. The RNAi effect was assessed 10 dpi by RT-qPCR. *Arabidopsis* roots were then collected and washed carefully at 35 dpi. Nematodes (parasitic juveniles at any stages and females) were stained by the sodium hypochlorite-acid fuchsin method (Bybd *et al.*, 1983). Nematodes, galls and egg masses were counted under a stereomicroscope microscope (Olympus, Japan). Three independent replicates were performed for each experiment, with counting on 30 plants of each line in each replicate.

Subcellular localisation and bimolecular fluorescence complementation (BiFC)

MiPDI1 woSP was amplified by PCR with specific Gateway primers (Table S1) and inserted into the pDONR207 donor vector. It was inserted into the pK7WGF2 (N-terminus eGFP) vector by recombination, with Gateway technology (Invitrogen). The *SlCYP* woSP and *SlSAP12* ORFs were inserted into the pK7WGR2 (N-terminus RFP) vector by recombination. For the BiFC assay, MiPDI1 was inserted into YFPn-, and SlSAP12 and SlCYP were inserted into YFPc-vectors (Walter *et al.*, 2004). The constructs were used to transform *A. tumefaciens* strain GV3101 or GV3301. Leaves from three- to four-week-old *N. tabacum* plants were subjected to agroinfiltration with recombinant strains of *A. tumefaciens,* as described by Zhao *et al*. (2019). Images were captured by confocal microscopy (Zeiss LSM880, Germany) at an excitation wavelength of 488 nm for GFP or YFP and 561 nm for RFP.

Yeast two-hybrid (Y2H) and co-immunoprecipitation (Co-IP) assay

For the Y2H screens, MiPDI1 woSP or a mutated version, MiPDI1-mu (the first CGHC activation site mutated to CGHG), was amplified (Table S1) and inserted into pB27 as a C-terminal fusion to LexA. The constructs were verified by sequencing and used to transform a L40ΔGal4 (matα) yeast strain. These baits were used to screen a random-primed cDNA library made from tomato roots infected with *M. incognita* and *Ralstonia solanacearum* in the Y187 (matα) yeast strain (Hybrigenics Services, Paris, France), by a mating approach. Diploids

displaying interactions were selected on a medium lacking tryptophan, leucine and histidine. The prey fragments of the positive clones were amplified by PCR and sequenced. The resulting sequences were used to identify the tomato interacting proteins with the Sol Genomics Network (https://solgenomics.net/) blast analysis tools. Pairwise Y2H assays were conducted following the instruction of Clontech protocol (Clontech, USA). Briefly, the *MiPDI1* coding region without the predicted signal peptide sequence was cloned into the pGBKT7 vector as the bait. The sequences encoding the SAP12 (SlSAP12, NbSAP12 and AtSAP12) were cloned into the pGADT7 vector as the preys. After co-transformation of yeast (Y2HGOLD) and screening on SD/-Leu-Trp plates, positive clones were verified and selected to grow on SD/-Leu-Trp-His medium with 0.5 mM 3-Amino-1,2,4-Triazole (3AT).

For Co-IP assays, the *MiPDI1*, *SlSAP12*, and *SlCYP* sequences were inserted into the PVX vector pGR107 with a FLAG-tag fused at the N-terminus (FLAG-MiPDI1) or an HA-tag fused at the C-terminus (SlSAP12-HA and SlCYP-HA) (Zhao *et al.*, 2019) and the resulting constructs were used to transform *A. tumefaciens* GV3101, which was then used to transform *N. tabacum* leaves. Total proteins were extracted from *N. tabacum* leaves. Co-IP was performed with anti-FLAG M2 affinity gel resin (Sigma-Aldrich, USA), according to the manufacturer's instructions. Briefly, the gel resin was washed twice with 1 ml ice-cold PBS. We then immediately added 1 ml of protein solution and incubated the mixture at 4°C for 4 h. The resin was thoroughly washed 5 times with 1 ml of ice-cold PBS, and then the proteins were eluted for western blot analysis. Anti-FLAG antibody (1:5000) and anti-HA (1:5000) antibodies (MBL, Japan) were incubated with the blot for protein detection.

Virus-induced gene silencing (VIGS)

VIGS assays were performed on *N. benthamiana*. The *N. benthamiana* orthologues of *SlSAP12* and *SlCYP* were identified in https://solgenomics.net. Regions for targeted gene silencing of *NbSAP12_Niben101Scf06280g06001/Niben101Scf06013g06013* and *NbCYP_Niben101Scf12813g00004* were identified with the Sol Genomics Network VIGS-Tool (Fernandez-Pozo *et al.*, 2015). Specific fragments were amplified by PCR with the primer pairs

TRV2-SAP12-F/TRV2-SAP12-R, and TRV2-CYP-F/TRV2-CYP-R (Table S1). The PCR products were digested with *Eco*RI and *Xho*I, and ligated to the tobacco rattle virus RNA 2 vector (TRV2) for transformation of the *A. tumefaciens* strain GV3101. VIGS assays were performed as previously described, by the infiltration of agrobacterial strains containing RNA 1 vector (TRV1) or TRV2 into leaves (Velasquez *et al.*, 2009; Lange *et al.*, 2013). The phytoene desaturase (*PDS*) gene was used as a positive control to check for successful gene silencing, which results in typical photobleaching symptoms on young growing leaves. Empty TRV2 and TRV1 were used as negative controls. One-week post-agroinfiltration, TRV-infected plants were inoculated with 200 *M. incognita* J2s. One-week later, five plants were used for RT-qPCR to assess the efficacy of gene silencing. Galls and females producing egg masses were counted 50 dpi.

Protein extraction, SDS-PAGE and western blotting

Total protein was extracted from agro-infiltrated *N. tabacum* leaves 2 dpi, with a protein extraction kit (Beijing ComWin Biotech Co., Ltd., China), according to the manufacturer's instructions. Briefly, 0.1 g of plant material was ground in liquid nitrogen and added to 0.5 ml of protein extraction buffer supplemented with the protease inhibitor PMSF (Sigma). Samples were kept on ice for 30 min, centrifuged at 12,000 rpm for 20 min at 4°C, and the protein was obtained in the supernatant. Proteins were fractionated by sodium dodecyl sulphate polyacrylamide gel electrophoresis (SDS-PAGE). For western blotting, an anti-MiPDI1 primary antibody was added to TBST (TBS with 0.1% Tween 20, 1% nonfat dry milk) at a ratio of 1: 6000. The membrane was then incubated with a secondary antibody directed against GFP (ABclonal, China), a FLAG-HRP antibody or an HA-HRP antibody (MBL, Japan), at a dilution of 1: 10000. Proteins were detected with the eECL Western Blot Kit (Beijing ComWin Biotech Co., Ltd., China).

Statistical analysis

The data were subjected to one-way ANOVA with Dunnett's multiple comparisons test or two-

way ANOVA with Tukey's multiple comparisons test. Statistical computations were carried out using GraphPad Prism (GraphPad Software Inc, La Jolla, CA, USA).

Accession numbers

All accession numbers are provided in Table S2. The GenBank accession numbers of *M. incognita* PDI sequences are MT370326 (MiPDI1), MT370324 (MiPDI2a) and MT370327 (MiPDI2b).

Results

Identification of secreted *M. incognita* PDIs

Using *M. incognita* genome and transcriptome datasets (Abad *et al.*, 2008; Nguyen *et al.*, 2018), we identified MiPDI1 (Minc07853a / MT370326) and MiPDI2 (MiPDI2a / Minc12006 / MT370324 and MiPDI2b / Minc15047 / MT370327, which are 99% identical). Sequence analysis showed that MiPDI1 and MiPDI2s contained the PDI structures common to other PDI-like proteins: four thioredoxin (Trx) domains (two activation sites in the first and fourth domains) and a N-terminal signal peptide (Fig. 1a). MiPDI1 was identified in previous *M. incognita* J2 secretome and female proteome studies, whereas MiPDI2 was detected only among female oesophageal gland proteins (Bellafiore *et al.*, 2008; Wang *et al.*, 2012).

Multiple sequence alignment and phylogenetic analysis were performed with PDI protein sequences from *M. incognita*, *M. graminicola* (MgPDI), *H. schachtii* (HsPDI), the free-living nematode *Caenorhabditis elegans* (CePDI1, CePDI2 and CePDI3), and the animal parasites *Brugia malayi* (BmPDI) and *Phytophthora parasitica* PpPDI1 (Fig. 1b, c). Two subgroups were identified in the tree; MiPDI2a/b was found to be more similar to the recently described HsPDI and MgPDI, whereas MiPDI1 formed a subgroup with CePDI1, CePDI2 and BmPDI (Fig. 1c). These results suggest that MiPDI1 is a new PDI-like protein that could potentially act as an effector of *M. incognita*.

MiPDI1 is expressed in the subventral oesophageal glands and upregulated in the parasitic

stages of *M. incognita*

The distribution of *MiPDI1* transcripts was investigated by ISH in preparasitic *M. incognita* J2s (pre-J2s). A specific signal was detected in subventral oesophageal gland cells after hybridisation with the digoxigenin-labelled MiPDI1 antisense probe (Fig. 2a; Fig. S1). No signal was detected in pre-J2s with sense negative controls (Fig. 2b).

The transcription of *MiPDI1* was analysed by RT-qPCR at various stages of *M. incognita* development. *MiPDI1* was significantly more strongly expressed in parasitic juveniles (Par-J 5 and 15 dpi) and females (Fig. 2c) than in pre-J2 and eggs. Together, these findings suggest that *MiPDI1* may play an important role in nematode parasitism in the plant.

MiPDI1 is secreted into plant tissues during parasitism

We performed immunolocalisation to determine whether and where MiPDI1 was secreted in host roots. A specific anti-MiPDI1 antibody was produced and a single band was detected in total protein samples from female pre-J2s, at the expected size of 57 kDa, corresponding to MiPDI1 without its signal peptide, and from *N. tabacum* leaves expressing MiPDI1-FLAG (Fig. S2). No signal was detected in protein samples from uninfected tomato roots, tomato leaves, *N. tabacum* and *N. benthamiana* leaves (Fig. S2). Immunolocalisation showed that the MiPDI1 protein was present in the subventral glands of pre-J2s (Fig. 2d,e), consistent with the ISH results. Immunohistochemistry on tomato gall sections at 5 and 10 dpi showed that MiPDI1 was present in the parasitic juveniles, at the stylet tip, and in the apoplast at early stages of infection (Fig. 2f,g; Fig. S3). In a number of gall sections containing nematodes, MiPDI1 was detected in both the anterior part of the nematode, along the cell wall of adjacent giant cells and in the giant cells (Fig. 2h,i,j; Fig. S3). No signal was observed in tomato gall sections incubated with pre-immune serum (Fig. S3). These results provide evidence for the secretion of the MiPDI1 effector *in planta* during parasitism.

Host-derived RNAi silencing and ectopic expression of *MiPDI1* shows the importance for *M. incognita* parasitism

We investigated the role of *MiPDI1* in *M. incognita* parasitism, through the use of host-derived RNAi to silence *MiPDI1* in feeding nematodes. Three T3 homozygous pdi-Ri *Arabidopsis* lines (pdi-1, pdi-3 and pdi-5) transformed with the *MiPDI1* hairpin dsRNA were obtained and infected with *M. incognita*. RT-qPCR analysis of *MiPDI1* in parasitic juveniles (10 dpi) showed much lower levels of *MiPDI1* expression (about 60%) in the three T3 pdi-Ri lines than in the control (WT and gfp-Ri) lines (Fig. 3a). Four weeks post infection, pdi-Ri lines presented significantly smaller numbers of galls and parasitic nematodes in the roots (Fig. 3b,c).

Two independent *Arabidopsis* lines ectopically expressing *MiPDI1* were generated, in which expression was induced by 30 µM dexamethasone (DEX). *MiPDI1*-expressing leaves showed some necrosis spots after they were sprayed with DEX (Fig. S4). The susceptibility to nematode infection of these two transgenic *Arabidopsis* lines was then determined. Both these transgenic lines were more susceptible ($P < 0.05$) to *M. incognita* infection than wild-type *Arabidopsis* (WT) after 35 dpi (Fig. 3d). Thus, the data for MiPDI1 silencing and overexpression provide evidence for a key role of MiPDI1 in *M. incognita* parasitism.

MiPDI1 interacts with SlSAP12, a stress-associated AN1-type zinc finger protein

We searched for host proteins interacting with MiPDI1 in two independent yeast two-hybrid analyses. We used the *MiPDI1* CDS without the signal peptide, or a form with a mutated first active site as baits to screen a tomato root cDNA library. In total, 7.5 and 26.7 million interactions were tested, respectively, leading to the identification of 13 proteins interacting with MiPDI1 and six proteins interacting with the mutated form (Table S3). The preys captured several times included two zinc finger proteins, a RING-type protein (Solyc03g026060), the AN1-type Stress-Associated Protein 12 (SlSAP12; Solyc02g087210), and two eukaryotic thiol proteases or cysteine proteases displaying 72.4% identity (Solyc04g078540 and Solyc12g088670). Interestingly, the SlSAP12 protein and one cysteine protease (Solyc04g078540, referred to hereafter as SlCYP) were identified in both independent screens, and were thus studied further. Reciprocal BLASTP showed that Solyc02g087210 was an orthologue of AtSAP12. Both these small cysteine-rich proteins (10%) are AN1-type SAPs,

containing only two AN1 zinc-finger domains, and 16 conserved cysteine residues (Fig. S5). Pairwise yeast two-hybrid assays with full-length proteins confirmed the interaction between SlSAP12 or SlCYP and MiPDI1 in yeast (Fig. 4a). Subcellular localisation studies involving agroinfiltration in *N. tabacum* showed a cytoplasmic localisation of RFP-SlCYP and MiPDI1-GFP and a nucleo-cytoplasmic localisation of RFP-SlSAP12 in epidermal cells (Fig. 4b). We also investigated the interaction of MiPDI1 with SlCYP and SlSAP12 *in planta* in bimolecular fluorescence complementation (BiFC) assays. The co-expression of YFPn-MiPDI1 and SlSAP12-YFPc reconstituted YFP fluorescence signals in the cytoplasm of *N. tabacum* epidermal cells (Fig. 4c, Fig. S6). We also performed co-immunoprecipitation (Co-IP) experiments to check the interaction between MiPDI1 and SlCYP or SlSAP12. MiPDI1 interacted with SlSAP12 in *N. tabacum*, further confirming the association of these two proteins *in planta* (Fig. 4d). By contrast, no interaction was detected between MiPDI1 and SlCYP, by either BiFC or Co-IP (Fig. 4c,d). These results confirm the specific interaction of MiPDI1 with SlSAP12 in plant cells.

SAP12 affects *M. incognita* parasitism

We further investigated the role of SAP12 in mediating the response to *M. incognita*, by silencing the *N. benthamiana SAP12* genes (*Niben101Scf06280g06001* and *Niben101Scf06013g06013* named *NbSAP12s*) or *CYP* (*Niben101Scf12813g00004,* named *NbCYP*) by virus-induced gene silencing (VIGS) (Table S2, Fig. S7). Quantitative RT-PCR analysis of the expression of the targeted homologous genes showed that *NbSAP12s* and *NbCYP* were downregulated (55-60%) in the plants subjected to VIGS relative to control plants (Fig. 5a; Fig. S7). *NbSAP12* silencing led to an increase in the number of females producing egg masses relative to the empty TRV2 control, whereas no significant effect was observed with *NbCYP* silencing (Fig. 5b). Finally, we tested a knockout T-DNA insertional mutant for *AtSAP12* (*AT3G28210*) (Fig. S8). The number of females producing egg masses and the number of galls were larger in homozygous *Arabidopsis* knockout (KO) *sap12* plants (*Salk_014706*) than in wild-type plants (Fig. 5c). These results indicate that SAP12 proteins

may play a role in plant - *M. incognita* interaction in Solanaceae and *Arabidopsis*.

***MiPDI1* expression in *Arabidopsis* affects stress- and defence-associated gene expression**

We investigated the effects of *MiPDI1* expression and *sap12* mutation on stress tolerance in *Arabidopsis*. We analysed genes involved in antioxidative functions (*AtCSD1* and *AtCSD2;* (Ma *et al.*, 2015), and responses to abiotic (*AtCOR47*, *AtRAB18* and *AtDH1;* (Kothari *et al.*, 2016) and biotic (*AtEM6*, *AtPR1a*, *AtPDF1.2a*, *AtPR4* and *AtPR1a;* (Qiu *et al.*, 2008; Aslam *et al.*, 2009; Rodiuc *et al.*, 2016; Kang *et al.*, 2017; Chang *et al.*, 2018) stresses in Arabidopsis. Four genes (*AtCSD2, AtEM6, AtRAB18* and the salicylic acid (SA) marker *AtPR1a*) were expressed less strongly in MiPDI1-overexpressing *Arabidopsis* plants, whereas the levels of expression of jasmonate (JA) and the ethylene markers PDF1.2a and PR4 were much higher in these plants (Fig. 5d). The expression of six genes (*AtCSD1*, *AtCSD2*, *AtDH1*, *AtPDF1.2a*, *AtPR4* and *AtPR1a*) was upregulated in the *sap12* KO line, whereas the stress-related genes *AtCOR47*, *AtRAB18* and *AtEM6* were downregulated (Fig. 5d). These results suggest that both MiPDI and its target may be responsible for regulating the expression of genes involved in stress responses to RKNs.

Discussion

The repertoire of putative nematode effectors is extremely large, and these molecules have been shown to manipulate many host plant functions to orchestrate the suppression of plant defences and the formation of specialised feeding cells (Mejias *et al.*, 2019). However, few data are available concerning the functions of effectors and few plant targets have been characterised, particularly for RKN effectors. Analyses of the secretomes of plant-parasitic nematodes and animal-parasitic nematodes have provided compelling evidence for the secretion of redox-regulated proteins, such as Trx, glutathione peroxidases, glutathione-S-transferases and PDIs (Bellafiore *et al.*, 2008; Hewitson *et al.*, 2008). PDIs are involved in the oxidoreduction and isomerisation of protein disulphide bonds, hydroxylation and protein deglutathionylation (Selles *et al.*, 2011; Ali Khan & Mutus, 2014). Recent studies have shown that *H. schachtii* and *M.*

graminicola PDI genes are expressed in the subventral glands of preparasitic J2s and upregulated in parasitic J2s. Functional studies have shown that these PDIs, which belong to the same subgroup as MiPDI2, play important roles in nematode parasitism through ROS detoxification (Habash *et al.*, 2017; Tian *et al.*, 2019). We characterised the role of a secreted *M. incognita* MiPDI1 effector identified in J2 secretome (Bellafiore *et al.*, 2008; Hewitson *et al.*, 2008) and identified its target in plant-RKN interactions, a stress-associated protein.

MiPDI1 is secreted throughout parasitism and targets the giant cells *in planta*

MiPDI1 transcript abundance increased significantly throughout parasitic stages *in planta* (from juveniles to females). We demonstrated that MiPDI1 was produced in the subventral oesophageal gland and secreted *in planta*, both in the apoplast during nematode migration, but also within the giant cells. Although the SvGs have been shown to be more active in the early stage of parasitism (Davis *et al.*, 2000), SvGs remain active *in planta* and produce effectors showing an increase in transcript abundance in parasitic juvenile stages compared to preparasitic J2s (Nguyen *et al.*, 2018). The secretion of MiPDI1 by SvGs would thus allow its production from the migration step to the formation of giant cells. Recent studies showed two PDI-like proteins of PPNs, MgPDI and HsPDI, were localised to the apoplast when GFP fusions were transiently expressed in *N. benthamiana* (Habash *et al.*, 2017; Tian *et al.*, 2019), indicating their different functional mechanism during nematode parasitism. Despite the hundreds of effectors characterised (Mejias *et al.*, 2019), few RKN effectors have been demonstrated to be secreted *in planta* and to target giant cells. Example of effectors are the *M. incognita* Mi-EFF1 (Jaouannet *et al.*, 2012) and MiMIF-2 (Zhao *et al.*, 2019), the *M. javanica* MjNULG1a (Lin *et al.*, 2016) and the *M. graminicola* MgGPP (Chen *et al.*, 2017) and Mg16820 (Naalden *et al.*, 2018). We also showed that the silencing of MiPDI1 *in planta* affected the number of galls and egg masses obtained and delayed nematode development. Accordingly, ectopic *MiPDI1* expression in *Arabidopsis* increased susceptibility to *M. incognita*. These results provide evidence that MiPDI1 is a novel plant-parasitic effector playing an essential role in nematode parasitism. In light of essential roles of PDI-like proteins

in redox regulation and mediating pathogens entry in infectious disease (Parakh & Atkin, 2015), MiPDI1 may protect parasitic nematode stages and feeding cells from oxidative stress. Indeed, studies of antioxidant molecule depletion have shown that the control of plant cell redox status is a key regulator of giant cell effectiveness (Baldacci-Cresp *et al.*, 2012).

MiPDI1 targets the redox-regulated stress-associated SAP12 proteins in *Arabidopsis* and Solanaceae

We further investigated the function of MiPDI1 in host cells, by searching for the proteins interacting with MiPDI1 in tomato. The putative targets identified included cysteine proteases and stress-associated zinc finger proteins, the activities of which are regulated by thiols/cysteines. Interestingly, the two cysteine proteases (SlCYPs) displaying high levels of sequence identity captured in our Y2H screen are orthologous to *Arabidopis* RD21a, a known target of the *M. chitwoodi* effector Mc01194 (Davies *et al.*, 2015). Cysteine proteases have a thiol group in the active site of the enzyme and are known to interact with Trx proteins (Montrichard *et al.*, 2009). PDI-like proteins have been shown to regulate RD21a activity in *Arabidopsis* (Andeme Ondzighi *et al.*, 2008), but we were unable to confirm the interaction of MiPDI1 with SlCYP in plant cells. The silencing of NbCYP in *N. benthamiana* did not affect plant susceptibility to *M. incognita,* suggesting that these molecules are not functional targets of MiPDI1.

The interaction of MiPDI1 with the tomato stress-associated protein SlSAP12, an AN1-type zinc finger protein was confirmed by Y2H, BiFC *in planta* and co-immunoprecipitation experiments. *SlSAP12* has been shown to be upregulated at later stages of gall formation in tomato, in response to *M. incognita* attack (Shukla *et al.*, 2018). The cysteine residues of zinc finger proteins are involved in zinc binding. The association of cysteine residues with zinc may therefore be affected by Trx, with consequences for protein activity (Carter & Ragsdale, 2014). AtSAP12 is a protein that undergoes major reversible redox-dependent conformational changes, facilitating a rapid response to changing environmental conditions (Stroher *et al.*, 2009). Under oxidising conditions (H_2O_2), oxidised SAP12 forms high-molecular mass aggregates. By

contrast, DTT and Trx reduce the oligomeric/dimeric form of SAP12 to the monomeric form lacking intermolecular disulphide bridges. SAP12 acts as a redox sensor capable of undergoing changes in its oligomeric conformation as a function of cellular redox potential, thereby transmitting redox information to other cell components (Stroher *et al.*, 2009). MiPDI1, which contains two Trx domains, could potentially regulate the activity of SAP12 by controlling its oligomerisation state *in planta*.

SAP proteins play important roles in plant responses to abiotic and biotic stresses

SAPs, which contain the AN1 and/or A20 zinc-finger domains in rice, are known to respond rapidly to diverse abiotic stresses and to play important roles in plant responses to these stresses (Krishna *et al.*, 2003; Vij & Tyagi, 2008; Solanke *et al.*, 2009; Stroher *et al.*, 2009; Dixit *et al.*, 2018). Thirteen *SAP* genes have been described in tomato (Solanke *et al.*, 2009), 14 in *Arabidopsis* (Stroher *et al.*, 2009), 18 in rice (Vij & Tyagi, 2006) and 57 in *Brassica napus* (He *et al.*, 2019). Levels of *AtSAP12* and *SlSAP12* expression increase immediately in response to various abiotic stresses (Solanke *et al.*, 2009). Interestingly, the *Arabidopsis* microRNA miR408, a key component of abiotic stress responses, is upregulated at 7 and 14 dpi in galls induced by *M. incognita* (Medina *et al.*, 2018). Higher levels of miR408 expression are associated with better tolerance to oxidative stress (Ma *et al.*, 2015). Cellular antioxidant capacity is enhanced in plants with high levels of miR408 expression, as demonstrated by the lower levels of reactive oxygen species and the induction of genes associated with antioxidative functions, such as *SAP12* (Ma *et al.*, 2015). In rice, *OsiSAP8* confers tolerance to abiotic stresses (Kanneganti & Gupta, 2008). Likewise, OsSAP1 plays important roles in the responses to both abiotic and biotic stresses, by interacting with aminotransferase (OsAMTR1) and the Pathogenesis-Related 1a Protein (OsSCP) (Tyagi *et al.*, 2014; Kothari *et al.*, 2016). AtSAP9 has been shown to mediate ABA signalling in response to biotic and abiotic stresses, possibly via the proteasome pathway (Kang *et al.*, 2017). Meanwhile, the plant A20-AN1 protein acts as a key hub, mediating antiviral immunity (Chang *et al.*, 2018). However, the modes of action of AN1-type proteins in plant pathogen responses remain largely unknown.

SlSAP3 and SlSAP4 have recently been shown to be positive regulators of immunity, to *Pseudomonas syringae* pv. tomato (Goldberger *et al.*) and *Botrytis cinerea* (Liu *et al.*, 2019a; Liu *et al.*, 2019b). SlSAP3 silencing decreased the Pst DC3000-induced expression of SA signaling and defense genes and attenuated immunity to Pst DC3000, whereas SlSAP3 overexpression in transgenic tomato increased them. We show here that *SAP12* silencing or knocking out *SAP12*, in *N. benthamiana* and in the *sap12* Arabidopsis mutant, respectively increased susceptibility to *M. incognita.* Moreover, the expression of some stress-associated marker genes was decreased in *MiPDI1*-expressing lines, whereas most of the genes investigated were upregulated in the *sap12* mutant. Thus, a dual function of MiPDI1 can hypothesized during plant–nematode interaction. MiPDI1 may contribute to *M. incognita* parasitism by protecting nematodes from oxidative stress during migration *in planta* and by interacting with SAP12 in the giant cells to fine-tune SAP12-mediated responses at the interface of redox signalling, defence and stress acclimation. One of the challenges for the future will be the establishment of assays for investigating the regulatory mechanism and showing how MiPDI1 and SAP12 orchestrate downstream responses.

Acknowledgments

We wish to thank Hybrigenics Services (Paris, France) for providing the pB27 and pP6 vectors, and the L40ΔGal4 and Y187 yeast strains, Dr Antony P. Page (University of Glasgow, UK) for providing an anti-CePDI-2 antibody we used in preliminary experiments and INRA SPE for financing Y2H library. J.M. benefits from a doctoral fellowship of the Ministère de l'Enseignement Supérieur, de la Recherche et de l'Innovation (MENRT grant). P.A., B.F., and M.Q. are supported by INRA and by the French Government (National Research Agency, ANR) through the 'Investments for the Future' LabEx SIGNALIFE: program reference #ANR-11-LABX-0028-01. This research supported by supported by the National Key Research and Development Program of China (No. 2017YFD0200601), the National Natural Science Foundation of China (Nos. 31571987, 31772138), and the National Basic Research Program of China (No. 2013CB127501). J.L.Z and C.Y.P got scholarships from China Scholarship Council

(No. 201606350083 and No. 201806350108) for studying in INRA, France.

Author contributions

JZ, JM and MQ designed, performed experiments and analysed the data. YC, ZM, QS, QL, BX performed experiments. JAE gave guidance for immunostaining. MQ, BX and PA supervised some of this work and provided input and expertise. HJ and BF were responsible for the development and guidance of the project. JZ, MQ, PA, BF and HJ wrote the manuscript with input from all co-authors.

References

Abad P, Gouzy J, Aury JM, Castagnone-Sereno P, Danchin EG, Deleury E, Perfus-Barbeoch L, Anthouard V, Artiguenave F, Blok VC, et al. 2008. Genome sequence of the metazoan plant-parasitic nematode *Meloidogyne incognita*. *Nature Biotechnology* **26**(8): 909-915.

Achour YB, Chenik M, Louzir H, Dellagi K. 2002. Identification of a Disulfide Isomerase Protein of *Leishmania major* as a Putative Virulence Factor. *Infection and Immunity* **70**(7): 3576-3585.

Ali Khan H, Mutus B. 2014. Protein disulfide isomerase a multifunctional protein with multiple physiological roles. *Frontiers in Chemistry* **2**: 70.

Andeme Ondzighi C, Christopher DA, Cho EJ, Chang SC, Staehelin LA. 2008. Arabidopsis protein disulfide isomerase-5 inhibits cysteine proteases during trafficking to vacuoles before programmed cell death of the endothelium in developing seeds. *Plant Cell* **20**(8): 2205-2220.

Aslam SN, Erbs G, Morrissey KL, Newman MA, Chinchilla D, Boller T, Molinaro A, Jackson RW, Cooper RM. 2009. Microbe-associated molecular pattern (MAMP) signatures, synergy, size and charge: influences on perception or mobility and host defence responses. *Molecular Plant Pathology* **10**(3): 375-387.

Baldacci-Cresp F, Chang C, Maucourt M, Deborde C, Hopkins J, Lecomte P, Bernillon S, Brouquisse R, Moing A, Abad P, et al. 2012. (Homo)glutathione deficiency impairs root-knot nematode development in *Medicago truncatula*. *PLoS Pathogens* **8**(1): e1002471.

Bellafiore S, Shen Z, Rosso MN, Abad P, Shih P, Briggs SP. 2008. Direct identification of the *Meloidogyne incognita* secretome reveals proteins with host cell reprogramming potential. *PLoS Pathogens* **4**(10): e1000192.

Blok VC, Jones JT, Phillips MS, Trudgill DL. 2008. Parasitism genes and host range disparities in biotrophic nematodes: the conundrum of polyphagy versus specialisation. *Bioessays* **30**(3): 249-259.

Bybd DW, Kirkpatrick T, Barker KR. 1983. An improved technique for clearing and staining plant tissues for detection of nematodes. *Journal of Nematology* **15**(1): 142-143.

Carter EL, Ragsdale SW. 2014. Modulation of nuclear receptor function by cellular redox poise. *Journal of Inorganic Biochemistry* **133**: 92-103.

Chang L, Chang HH, Chang JC, Lu HC, Wang TT, Hsu DW, Tzean Y, Cheng AP, Chiu YS, Yeh HH. 2018. Plant A20/AN1 protein serves as the important hub to mediate antiviral immunity. *PLoS Pathogens* **14**(9): e1007288.

Chen J, Hu L, Sun L, Lin B, Huang K, Zhuo K, Liao J. 2018. A novel *Meloidogyne graminicola* effector, MgMO237, interacts with multiple host defence-related proteins to manipulate plant basal immunity and promote parasitism. *Molecular Plant Pathology*.

Chen J, Lin B, Huang Q, Hu L, Zhuo K, Liao J. 2017. A novel *Meloidogyne graminicola* effector, MgGPP, is secreted into host cells and undergoes glycosylation in concert with proteolysis to suppress plant defenses and promote parasitism. *PLoS Pathogens* **13**(4): e1006301.

Dafny-Yelin M, Chung SM, Frankman EL, Tzfira T. 2007. pSAT RNA interference vectors: a modular series for multiple gene down-regulation in plants. *Plant Physiology* **145**(4): 1272-1281.

Davies LJ, Elling AA, Zhang L. 2015. The *Arabidopsis thaliana* papain-like cysteine protease RD21 interacts with a root-knot nematode effector protein. *Nematology* **17**(6): 655-666.

Davis EL, Hussey RS, Baum TJ, Bakker J, Schots A, Rosso MN, Abad P. 2000. Nematode Parasitism Genes. *Annual Review of Phytopathology* **38**: 365-396.

de Almeida Engler J, Van Poucke K, Karimi M, De Groodt R, Gheysen G, Engler G, Gheysen G. 2004. Dynamic cytoskeleton rearrangements in giant cells and syncytia of nematode-infected roots. *The Plant Journal* **38**(1): 12-26.

Dixit A, Tomar P, Vaine E, Abdullah H, Hazen S, Dhankher OP. 2018. A stress-associated protein, AtSAP13, from *Arabidopsis thaliana* provides tolerance to multiple abiotic stresses. *Plant, Cell & Environment* **41**(5): 1171-1185.

Favery B, Quentin M, Jaubert-Possamai S, Abad P. 2016. Gall-forming root-knot nematodes hijack key plant cellular functions to induce multinucleate and hypertrophied feeding cells. *Journal of Insect Physiology* **84**: 60-69.

Fernandez-Pozo N, Menda N, Edwards JD, Saha S, Tecle IY, Strickler SR, Bombarely A, Fisher-York T, Pujar A, Foerster H, et al. 2015. The Sol Genomics Network (SGN)--from genotype to phenotype to breeding. *Nucleic Acids Research* **43**(Database issue): D1036-1041.

Goldberger RF, Epstein CJ, Anfinsen CB. 1963. Acceleration of reactivation of reduced bovine pancreatic ribonuclease by a microsomal system from rat liver. *Journal of Biological Chemistry* **238**: 628-635.

Habash SS, Sobczak M, Siddique S, Voigt B, Elashry A, Grundler FMW. 2017. Identification and characterization of a putative protein disulfide isomerase (HsPDI) as an alleged effector of *Heterodera schachtii*. *Scientific Reports* **7**(1): 13536.

Han H, Dong H, Zhu S, Zhao Q, Jiang L, Wang Y, Li L, Wu Y, Huang B. 2014. Molecular characterization and analysis of a novel protein disulfide isomerase-like protein of

Eimeria tenella. *PloS One* **9**(6): e99914.

He X, Xie S, Xie P, Yao M, Liu W, Qin L, Liu Z, Zheng M, Liu H, Guan M, et al. 2019. Genome-wide identification of stress-associated proteins (SAP) with A20/AN1 zinc finger domains associated with abiotic stresses responses in *Brassica napus*. *Environmental and Experimental Botany* **165**: 108-119.

Hewitson JP, Harcus YM, Curwen RS, Dowle AA, Atmadja AK, Ashton PD, Wilson A, Maizels RM. 2008. The secretome of the filarial parasite, *Brugia malayi*: proteomic profile of adult excretory-secretory products. *Molecular and Biochemical Parasitology* **160**(1): 8-21.

Huang G, Dong R, Allen R, Davis EL, Baum TJ, Hussey RS. 2006. A root-knot nematode secretory peptide functions as a ligand for a plant transcription factor. *Molecular Plant-Microbe Interactions* **19**(5): 463-470.

Jaouannet M, Nguyen C-N, Quentin M, Jaubert-Possamai S, Rosso M-N, Favery B. 2018. *In situ* Hybridization (ISH) in Preparasitic and Parasitic Stages of the Plant-parasitic Nematode *Meloidogyne* spp. *Bio-Protocol* **8**(6).

Jaouannet M, Perfus-Barbeoch L, Deleury E, Magliano M, Engler G, Vieira P, Danchin EG, Da Rocha M, Coquillard P, Abad P, et al. 2012. A root-knot nematode-secreted protein is injected into giant cells and targeted to the nuclei. *New Phytologist* **194**(4): 924-931.

Jaubert S, Ledger TN, Laffaire JB, Piotte C, Abad P, Rosso MN. 2002. Direct identification of stylet secreted proteins from root-knot nematodes by a proteomic approach. *Molecular and Biochemical Parasitology* **121**(2): 205-211.

Jaubert S, Milac AL, Petrescu AJ, de Almeida-Engler J, Abad P, Rosso MN. 2005. In planta secretion of a calreticulin by migratory and sedentary stages of root-knot nematode. *Molecular Plant-Microbe Interactions* **18**(12): 1277-1284.

Kang M, Lee S, Abdelmageed H, Reichert A, Lee HK, Fokar M, Mysore KS, Allen RD. 2017. Arabidopsis stress associated protein 9 mediates biotic and abiotic stress responsive ABA signaling via the proteasome pathway. *Plant, Cell & Environment* **40**(5): 702-716.

Kanneganti V, Gupta AK. 2008. Overexpression of *OsiSAP8*, a member of stress associated protein (SAP) gene family of rice confers tolerance to salt, drought and cold stress in transgenic tobacco and rice. *Plant Molecular Biology* **66**(5): 445-462.

Kothari KS, Dansana PK, Giri J, Tyagi AK. 2016. Rice Stress Associated Protein 1 (OsSAP1) Interacts with Aminotransferase (OsAMTR1) and Pathogenesis-Related 1a Protein (OsSCP) and Regulates Abiotic Stress Responses. *Frontiers in Plant Science* **7**: 1057.

Krishna SS, Majumdar I, Grishin NV. 2003. Structural classification of zinc fingers: survey and summary. *Nucleic Acids Research* **31**(2): 532-550.

Lange M, Yellina AL, Orashakova S, Becker A. 2013. Virus-induced gene silencing (VIGS) in plants: an overview of target species and the virus-derived vector systems. *Methods in Molecular Biology* **975**: 1-14.

Li Y, Williams B, Dickman M. 2017. Arabidopsis B-cell lymphoma2 (Bcl-2)-associated

athanogene 7 (BAG7)-mediated heat tolerance requires translocation, sumoylation and binding to WRKY29. *New Phytol* **214**(2): 695-705.

Liao M, Hatta T, Umemiya R, Huang P, Jia H, Gong H, Zhou J, Nishikawa Y, Xuan X, Fujisaki K. 2007. Identification of three protein disulfide isomerase members from *Haemaphysalis longicornis* tick. *Insect Biochemistry and Molecular Biology* **37**(7): 641-654.

Lin B, Zhuo K, Chen S, Hu L, Sun L, Wang X, Zhang LH, Liao J. 2016. A novel nematode effector suppresses plant immunity by activating host reactive oxygen species-scavenging system. *New Phytologist* **209**(3): 1159-1173.

Liu S, Wang J, Jiang S, Wang H, Gao Y, Zhang H, Li D, Song F. 2019a. Tomato SlSAP3, a member of the stress-associated protein family, is a positive regulator of immunity against *Pseudomonas syringae* pv. tomato DC3000. *Molecular Plant Pathology* **20**(6): 815-830.

Liu S, Yuan X, Wang Y, Wang H, Wang J, Shen Z, Gao Y, Cai J, Li D, Song F. 2019b. Tomato Stress-Associated Protein 4 Contributes Positively to Immunity Against Necrotrophic Fungus *Botrytis cinerea*. *Molecular Plant-Microbe Interactions* **32**(5): 566-582.

Livak KJ, Schmittgen TD. 2001. Analysis of relative gene expression data using real-time quantitative PCR and the 2(-Delta Delta C(T)) Method. *Methods* **25**(4): 402-408.

Ma C, Burd S, Lers A. 2015. *miR408* is involved in abiotic stress responses in Arabidopsis. *the Plant Journal* **84**(1): 169-187.

Mahajan B, Noiva R, Yadava A, Zheng H, Majam V, Mohan KV, Moch JK, Haynes JD, Nakhasi H, Kumar S. 2006. Protein disulfide isomerase assisted protein folding in malaria parasites. *International Journal for Parasitology* **36**(9): 1037-1048.

Medina C, da Rocha M, Magliano M, Raptopoulo A, Marteu N, Lebrigand K, Abad P, Favery B, Jaubert-Possamai S. 2018. Characterization of siRNAs clusters in *Arabidopsis thaliana* galls induced by the root-knot nematode *Meloidogyne incognita*. *BMC Genomics* **19**(1): 943.

Mejias J, Truong NM, Abad P, Favery B, Quentin M. 2019. Plant Proteins and Processes Targeted by Parasitic Nematode Effectors. *Frontiers in Plant Science* **10**: 970.

Meng Y, Zhang Q, Zhang M, Gu B, Huang G, Wang Q, Shan W. 2015. The protein disulfide isomerase 1 of *Phytophthora parasitica* (PpPDI1) is associated with the haustoria-like structures and contributes to plant infection. *Frontiers in Plant Science* **6**: 632.

Montrichard F, Alkhalfioui F, Yano H, Vensel WH, Hurkman WJ, Buchanan BB. 2009. Thioredoxin targets in plants: the first 30 years. *Journal of Proteomics* **72**(3): 452-474.

Naalden D, Haegeman A, de Almeida-Engler J, Birhane Eshetu F, Bauters L, Gheysen G. 2018. The *Meloidogyne graminicola* effector Mg16820 is secreted in the apoplast and cytoplasm to suppress plant host defense responses. *Molecular Plant Pathology* **19**(11): 2416-2430.

Nguyen CN, Perfus-Barbeoch L, Quentin M, Zhao J, Magliano M, Marteu N, Da Rocha M, Nottet N, Abad P, Favery B. 2018. A root-knot nematode small glycine and

cysteine-rich secreted effector, MiSGCR1, is involved in plant parasitism. *New Phytologist* **217**(2): 687-699.

Parakh S, Atkin JD. 2015. Novel roles for protein disulphide isomerase in disease states: a double edged sword? *Frontiers in Cell and Developmental Biology* **3**: 30.

Qiu JL, Zhou L, Yun BW, Nielsen HB, Fiil BK, Petersen K, Mackinlay J, Loake GJ, Mundy J, Morris PC. 2008. Arabidopsis mitogen-activated protein kinase kinases MKK1 and MKK2 have overlapping functions in defense signaling mediated by MEKK1, MPK4, and MKS1. *Plant Physiology* **148**(1): 212-222.

Rodiuc N, Barlet X, Hok S, Perfus-Barbeoch L, Allasia V, Engler G, Seassau A, Marteu N, de Almeida-Engler J, Panabieres F, et al. 2016. Evolutionarily distant pathogens require the Arabidopsis phytosulfokine signalling pathway to establish disease. *Plant, Cell & Environment* **39**(7): 1396-1407.

Selles B, Jacquot JP, Rouhier N. 2011. Comparative genomic study of protein disulfide isomerases from photosynthetic organisms. *Genomics* **97**(1): 37-50.

Shukla N, Yadav R, Kaur P, Rasmussen S, Goel S, Agarwal M, Jagannath A, Gupta R, Kumar A. 2018. Transcriptome analysis of root-knot nematode (*Meloidogyne incognita*)-infected tomato (*Solanum lycopersicum*) roots reveals complex gene expression profiles and metabolic networks of both host and nematode during susceptible and resistance responses. *Molecular Plant Pathology* **19**(3): 615-633.

Solanke AU, Sharma MK, Tyagi AK, Sharma AK. 2009. Characterization and phylogenetic analysis of environmental stress-responsive SAP gene family encoding A20/AN1 zinc finger proteins in tomato. *Molecular Genetics and Genomics* **282**(2): 153-164.

Stroher E, Wang XJ, Roloff N, Klein P, Husemann A, Dietz KJ. 2009. Redox-dependent regulation of the stress-induced zinc-finger protein SAP12 in *Arabidopsis thaliana*. *Molecular Plant* **2**(2): 357-367.

Tian ZL, Wang ZH, Maria M, Qu N, Zheng JW. 2019. *Meloidogyne graminicola* protein disulfide isomerase may be a nematode effector and is involved in protection against oxidative damage. *Scientific Reports* **9**(1): 11949.

Trifinopoulos J, Nguyen LT, von Haeseler A, Minh BQ. 2016. W-IQ-TREE: a fast online phylogenetic tool for maximum likelihood analysis. *Nucleic Acids Research* **44**(W1): W232-235.

Tyagi H, Jha S, Sharma M, Giri J, Tyagi AK. 2014. Rice SAPs are responsive to multiple biotic stresses and overexpression of OsSAP1, an A20/AN1 zinc-finger protein, enhances the basal resistance against pathogen infection in tobacco. *Plant Science* **225**: 68-76.

Velasquez AC, Chakravarthy S, Martin GB. 2009. Virus-induced gene silencing (VIGS) in *Nicotiana benthamiana* and tomato. *Jove-Journal of Visualized Experiments*(28).

Vieira P, Gleason C. 2019. Plant-parasitic nematode effectors - insights into their diversity and new tools for their identification. *Current Opinion in Plant Biology* **50**: 37-43.

Vij S, Tyagi AK. 2006. Genome-wide analysis of the stress associated protein (SAP) gene family containing A20/AN1 zinc-finger(s) in rice and their phylogenetic relationship with Arabidopsis. *Molecular Genetics and Genomics* **276**(6): 565-575.

748 **Vij S, Tyagi AK. 2008.** A20/AN1 zinc-finger domain-containing proteins in plants and animals
749 represent common elements in stress response. *Functional & Integrative Genomics* **8**(3):
750 301-307.
751 **Walter M, Chaban C, Schutze K, Batistic O, Weckermann K, Nake C, Blazevic D, Grefen**
752 **C, Schumacher K, Oecking C, et al. 2004.** Visualization of protein interactions in
753 living plant cells using bimolecular fluorescence complementation. *The Plant Journal*
754 **40**(3): 428-438.
755 **Wang XR, Moreno YA, Wu HR, Ma C, Li YF, Zhang JA, Yang C, Sun S, Ma WJ, Geary**
756 **TG. 2012.** Proteomic profiles of soluble proteins from the esophageal gland in female
757 *Meloidogyne incognita*. *International Journal for Parasitology* **42**(13-14): 1177-1183.
758 **Winter AD, Page AP. 2000.** Prolyl 4-hydroxylase is an essential procollagen-modifying
759 enzyme required for exoskeleton formation and the maintenance of body shape in the
760 nematode *Caenorhabditis elegans*. *Molecular and Cellular Biology* **20**(11): 4084-4093.
761 **Zhang X, Henriques R, Lin SS, Niu QW, Chua NH. 2006.** *Agrobacterium*-mediated
762 transformation of *Arabidopsis thaliana* using the floral dip method. *Nature Protocols*
763 **1**(2): 641-646.
764 **Zhao J, Li L, Liu Q, Liu P, Li S, Yang D, Chen Y, Pagnotta S, Favery B, Abad P, et al.**
765 **2019.** A MIF-like effector suppresses plant immunity and facilitates nematode
766 parasitism by interacting with plant annexins. *Journal of Experimental Botany* **70**(20):
767 5943-5958.

Fig. 1 Primary structure of MiPDIs. (a) Functional domains of MiPDI1 and MiPDI2. MiPDI1 and MiPDI2 have an N-terminal signal peptide for secretion, four thioredoxin domains (a, b, b', a') predicted by an NCBI conserved domain search, and two catalytic domains containing characteristic CGHC active sites in the a and a' domains. (b) A ClustalW2 alignment of the PDI-like proteins MiPDI1 and MiPDI2 (from *Meloidogyne incognita*), CePDI (*Caenorhabditis elegans*), HsPDI (*Heterodera schachtii*), MgPDI (*Meloidogyne graminicola*), BmPDI (*Brugia malayi*) and PpPDI (*Phytophthora parasitica*). Identical and highly similar (>75%) amino-acid residues are highlighted against black background shading, similar (>50%) amino-acid residues are shown in grey. Yellow background shading indicates the peptide used in the production of the polyclonal anti-MiPDI1 antibody. The sequences for active site CGHC motif are shown in the red frame. The four thioredoxin (TRX) domains are indicated. (c) Maximum likelihood phylogenetic tree of PDI sequences presented in (b). Support for the nodes was calculated with a hundred bootstrap replicates. PpPDI was used as the outgroup.

Fig. 2 Localisation and temporal expression pattern of MiPDI. (a) *In situ* hybridisation (ISH) of digoxigenin-labelled antisense *MiPDI1* probe to pre-parasitic *M. incognita* J2s, showing transcripts expressed in the subventral oesophageal gland (SvG). The stylet and the metacarpus are indicated. (b) ISH with the *MiPDI1* sense probe gave no signal. (c) Temporal pattern of *MiPDI1* expression. The relative level of *MiPDI1* expression throughout nematode development was quantified by RT-qPCR for five different *M. incognita* stages relative to the egg stage (means ±SE). Data were analysed by the $2^{-\Delta\Delta Ct}$ method. Different letters indicate statistically significant difference between each column using two-way ANOVA following Tukey's multiple comparisons test (P<0.05). Pre-J2: preparasitic second-stage juvenile; par-J: parasitic juveniles, including parasitic second-stage juveniles (5 dpi) and parasitic third- and fourth-stage juveniles (15 dpi). dpi: days post infection. (d-e) Immunolocalisation with the anti-MiPDI1 antibody showed that the MiPDI1 protein was present in the subventral oesophageal glands (SvG). (d) Overlay of images of the differential interference contrast and Alexa Fluor 488 fluorescence. (e) Alexa Fluor 488 fluorescence image. Bar: 20 µm. (f) Localisation of the

secreted MiPDI1 protein in the nematode anterior part (black arrow) and at the tip of the stylet (red arrow). (g) Localisation of the secreted MiPDI1 protein in the tip of the stylet and in plant tissue (red arrow). (h-j) MiPDI1 protein accumulated in the nematode anterior part (black arrow), the giant or plant cell wall (red arrows) and in the giant cell (yellow arrow). Micrographs f-j are overlays of images of the DIC, DAPI-stained nuclei and Alexa Fluor 488 fluorescence images. Individual images are presented in Figure S3. N, nematode; *, giant cell. m, metacorpus; Scale bar, 20 μm.

Fig. 3 The effect of host-derived RNA interference (RNAi) and ectopic expression of *M. incognita MiPDI1* in *Arabidopsis* on RKN infection. (a) *MiPDI1* expression in three independent, homozygous pdi-Ri lines, two gfp-RNAi lines and the wild type (WT) were determined 10 dpi by RT-qPCR. The data shown are means ±SE from three independent biological replicates. (b) Phenotypes of nematodes in different *Arabidopsis* line roots. Acid fuchsin was used to stain *Arabidopsis* roots after *M. incognita* infection 35 days. For each line, at least 10 roots were observed, and the experiment was repeated three times. Bars represent 300 μm. (c) *In vivo* RNAi of *MiPDI1* in *Arabidopsis* reduced the level of *M. incognita* infection. Mean numbers of galls and nematodes (parasitic juveniles at any stage and females) were determined at 35 dpi in various *Arabidopsis* lines. Data are presented as means ±SD ($n \geq 30$). Similar results were obtained in three independent experiments. One representative experiment is shown. (d) *MiPDI1* expression led to a reproducible increase in *Arabidopsis* susceptibility to *M. incognita*. Total numbers of egg masses in two independent *MiPDI1* transgenic lines were counted at 35 dpi. Two independent experiments were conducted for each line, and 30 plants were analysed per line. (a, c, d) Different letters indicate statistically significant difference in two-way ANOVA with Tukey's multiple comparisons test ($P<0.05$).

Fig. 4 MiPDI1 interacts with *Arabidopsis* and Solanaceae stress-associated proteins SAP12. (a) Pairwise yeast two-hybrid tests were performed to investigate the interactions between MiPDI1 and cysteine proteinase (SlCYP) or SAP12 proteins from *S. lycopersicum* (SlSAP12), *N.*

benthamiana (NbSAP12) and *A. thaliana* (AtSAP12). Left column, yeast cell growth carrying the baits (in pGBKT7 vector) and preys (in pGADT7) grown on SD/-trp-leu medium indicating successful transformation of the yeast with both plasmids; right column, yeast cell growth on the selective triple dropout medium (SD/-trp-leu-his) following the addition of 3-amino-1,2,4-triazole (3AT) indicating protein interaction. Yeast cells containing p53 and SV40 were used as positive control. (b) Subcellular localisation of MiPDI1, GFP-SlCYP and SlSAP12 in *N. benthamiana*. MiPDI1-eGFP, eGFP, SlCYP-RFP and SlSAP12-RFP were transiently expressed in *N. benthamiana* leaves. Signals were detected 48 h after infiltration. Images were captured by confocal microscopy (Zeiss LSM 880, Germany). Scale bar, 20 μm. (c) Bimolecular fluorescence complementation (BiFC) visualisation of the interaction between MiPDI1 and SlSAP12. *N. benthamiana* leaves were transformed with YFPn-MiPDI1 and SlSAP12-YFPc or SlCYP-YFPc. Images were obtained 36 h after co-expression. Signals were observed in the cytoplasm in leaves co-infiltrated with YFPn-MiPDI1 and SlSAP12-YFPc. (b, c) At least ten cells from three leaves of three different plants were observed with similar results. YFP, yellow fluorescent protein. Scale bar, 20 μm or 50 μm. (d) Co-immunoprecipitation (Co-IP) analysis of MiPDI1 interacting with SlSAP12. FLAG-MiPDI1 or FLAG-GFP was transiently co-expressed with SlSAP12-HA or SlCYP-HA in tobacco leaves. Co-IP was performed with anti-FLAG M2 affinity gel resin (Sigma-Aldrich), and the isolated protein was detected by western blotting with an anti-FLAG antibody to detect MiPDI1 or eGFP, and an anti-HA antibody to detect SlSAP12 or SlCYP. eGFP, enhanced green fluorescent protein.

Fig. 5 Effect on susceptibility to *M. incognita* of virus-induced gene silencing (VIGS) of *NbSAP12s* and *NbCYP* in *N. benthamiana*, and of the *A. thaliana sap12* knockout mutant. (a) Levels of *NbSAP12s* and *NbCYP* transcripts in *N. benthamiana* following silencing, as assessed by real-time quantitative PCR (RT-qPCR). Error bars represent the standard errors for 10 biological replicates, and the results of two independent experiments were presented. (b) *N. benthamiana* plants in which *NbSAP12s* was silenced were more susceptible to *M. incognita*, whereas those in which *NbCYP* was silenced were not significantly different from the wild type

in terms of susceptibility, as indicated by the mean numbers of egg masses on plant roots. Error bars represent the mean ± SD (n≥15). All experiments were performed twice, and at least 15 plants were analysed per treatment. (c) The *sap12* mutant line (*SALK_014706*) was more susceptible to *M. incognita*, as shown by the mean numbers of egg masses and galls in roots. Error bars represent the mean ± SD (n≥20). Two independent experiments were conducted and yielded similar results, with at least 30 plants analysed per treatment. (a, b, c) Different letters indicate statistically significant difference in two-way ANOVA with Tukey's multiple comparisons test (P <0.05). (d) Levels of expression for stress- and defence-related genes in MiPDI1-expressing lines (*MiPDI1-1* and *MiPDI1-2*), the *sap12* mutant line (*SALK_014706*) and the wild type (WT). The genes considered were *AtCSD1* (cytosolic Cu/Zn superoxide dismutase), *AtCSD2* (chloroplastic Cu/Zn superoxide dismutase), *AtCOR47* and *AtRAB18* (from the dehydrin protein family), *AtADH1* (catalysing the reduction of acetaldehyde with NADH as reductant), *AtEM6* (stress-induced protein), *AtNPR1* and *AtPR1a* (SA-mediated defence response marker gene), *AtPDF1.2a* (encoding ethylene- and jasmonate-responsive plant defences), *AtPR4* (ethylene-responsive pathogenesis-related protein). *AtOXA1* (AT5G62050) and *AtUBP22* (AT5G10790) were used as internal controls. Expression levels were measured by real-time quantitative PCR (RT-qPCR) and the data shown are means ±SD (n = 4). Asterisks indicate significant differences for single stress- and defence-related gene among different plant lines by one-way ANOVA with Dunnett's multiple comparisons test (*P < 0.05, ** P<0.01, *** P <0.001).

Supporting information

Table S1 Primers used in this study.

Table S2 Accession numbers used in this study.

Table S3 Yeast-two hybrid clones obtained using MiPDI1-mu or MiPDI1 as bait and corresponding gene expression in galls induced by *M. incognita*.

Fig. S1 MiPDI1 probe used for *in situ* hybridization (ISH).

Fig. S2 Western blot analysis verified specificity of MiPDI1 antibody.

774 **Fig. S3** Localization of MiPDI1 in tomato root gall sections during *M. incognita* parasitism.

775 **Fig. S4** Verification of homozygous *MiPDI1* ectopic expressing Arabidopsis lines by RT-PCR

776 and western blot.

777 **Fig. S5** Structure of AtSAP12, NbSAP12 and SlSAP12 proteins.

778 **Fig. S6** MiPDI1 could not interact with SlCYP *in planta* by using BiFC.

779 **Fig. S7** Characteristics of *SAP12* and *CYP* genes, and VIGS phenotypes.

Fig. S8 Verification of homozygous T-DNA insertion mutants of *AtSAP12*.

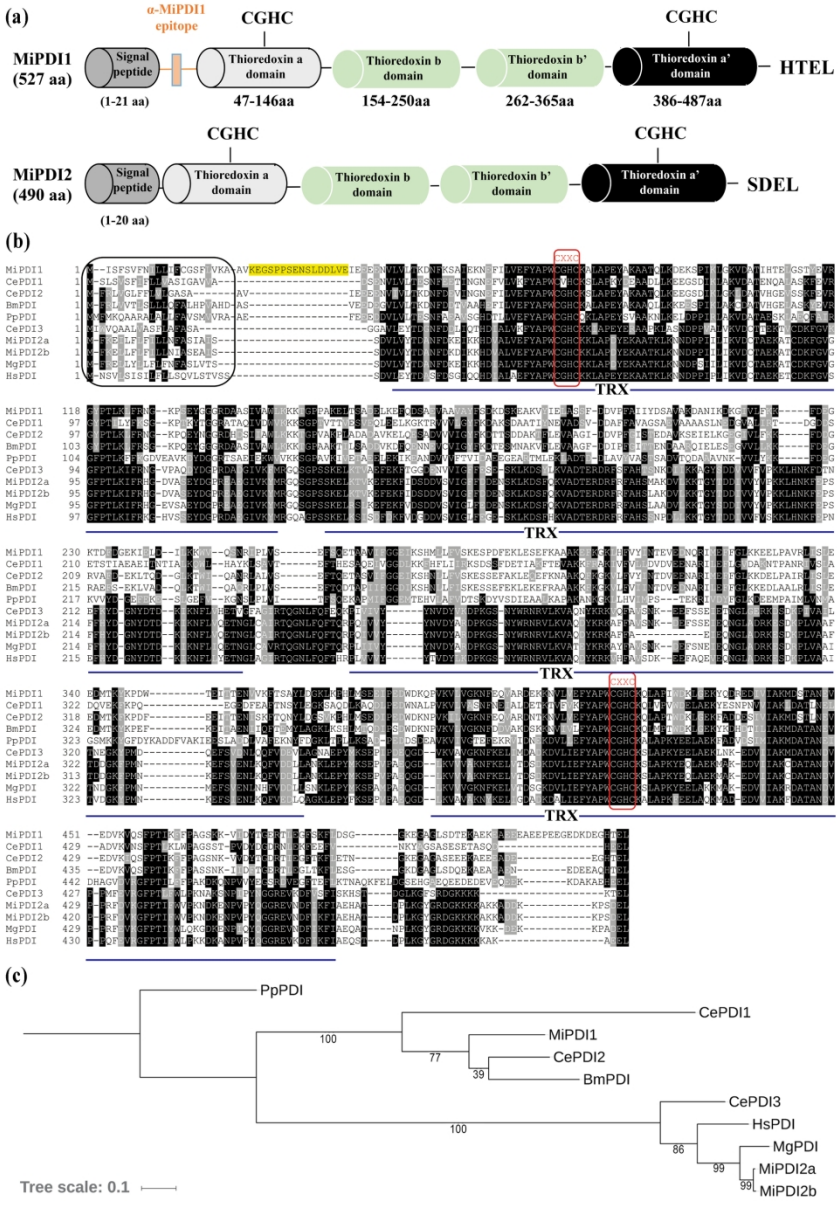

Fig. 1 Primary structure of MiPDIs. (a) Functional domains of MiPDI1 and MiPDI2. MiPDI1 and MiPDI2 have an N-terminal signal peptide for secretion, four thioredoxin domains (a, b, b', a') predicted by an NCBI conserved domain search, and two catalytic domains containing characteristic CGHC active sites in the a and a' domains. (b) A ClustalW2 alignment of the PDI-like proteins MiPDI1 and MiPDI2 (from Meloidogyne incognita), CePDI (Caenorhabditis elegans), HsPDI (Heterodera schachtii), MgPDI (Meloidogyne graminicola), BmPDI (Brugia malayi) and PpPDI (Phytophthora parasitica). Identical and highly similar (>75%) amino-acid residues are highlighted against black background shading, similar (>50%) amino-acid residues are shown in grey. Yellow background shading indicates the peptide used in the production of the polyclonal anti-MiPDI1 antibody. The sequences for active site CGHC motif are shown in the red frame. The four thioredoxin (TRX) domains are indicated. (c) Maximum likelihood phylogenetic tree of PDI sequences presented in (b). Support for the nodes was calculated with a hundred bootstrap replicates. PpPDI was used as the outgroup.

160x228mm (300 x 300 DPI)

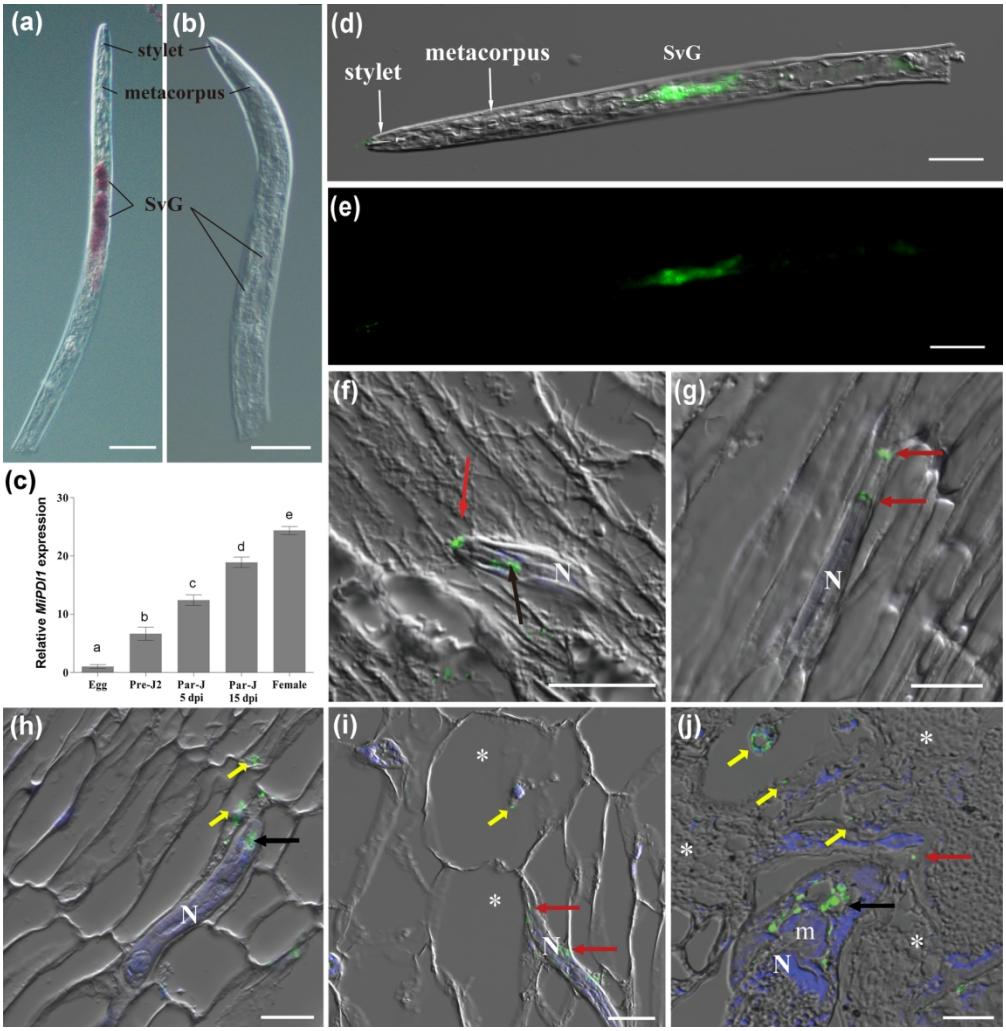

Fig. 2 Localisation and temporal expression pattern of MiPDI. (a) In situ hybridisation (ISH) of digoxigenin-labelled antisense MiPDI1 probe to pre-parasitic M. incognita J2s, showing transcripts expressed in the subventral oesophageal gland (SvG). The stylet and the metacarpus are indicated. (b) ISH with the MiPDI1 sense probe gave no signal. (c) Temporal pattern of MiPDI1 expression. The relative level of MiPDI1 expression throughout nematode development was quantified by RT-qPCR for five different M. incognita stages relative to the egg stage (means ±SE). Data were analysed by the 2-ΔΔCt method. Different letters indicate statistically significant difference between each column using two-way ANOVA following Tukey's multiple comparisons test ($P<0.05$). Pre-J2: preparasitic second-stage juvenile; par-J: parasitic juveniles, including parasitic second-stage juveniles (5 dpi) and parasitic third- and fourth-stage juveniles (15 dpi). dpi: days post infection. (d-e) Immunolocalisation with the anti-MiPDI1 antibody showed that the MiPDI1 protein was present in the subventral oesophageal glands (SvG). (d) Overlay of images of the differential interference contrast and Alexa Fluor 488 fluorescence. (e) Alexa Fluor 488 fluorescence image. Bar: 20 µm. (f) Localisation of the secreted MiPDI1 protein in the nematode anterior part (black arrow) and at the tip of the stylet (red arrow). (g) Localisation of the secreted MiPDI1 protein in the tip of the stylet and in plant tissue (red arrow). (h-j) MiPDI1 protein accumulated in the nematode anterior part (black arrow), the giant or plant cell wall (red arrows) and in the giant cell (yellow arrow). Micrographs f-j are overlays of images of the DIC, DAPI-stained nuclei and Alexa Fluor 488 fluorescence images. Individual images are presented in Figure S3. N, nematode; *, giant cell. m, metacorpus; Scale bar, 20 µm.

160x163mm (300 x 300 DPI)

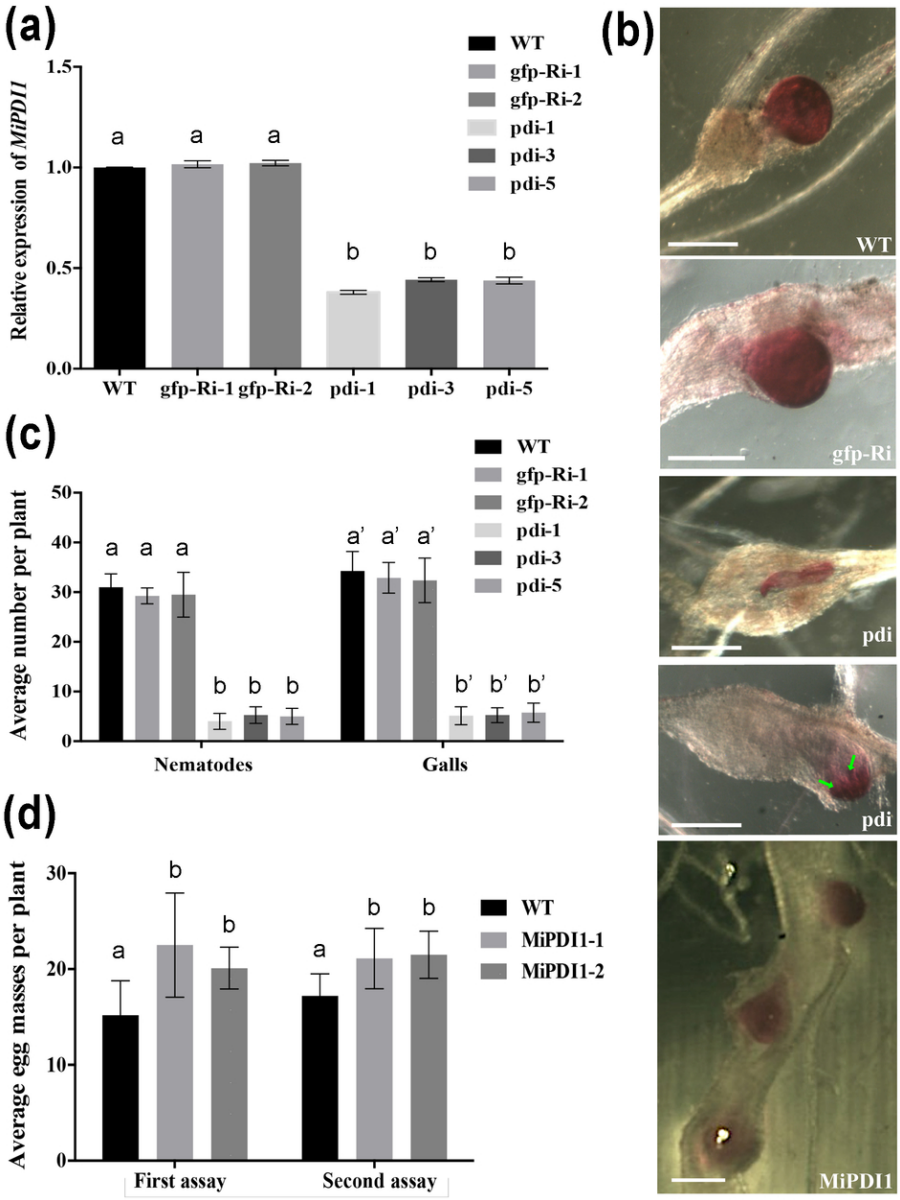

Fig. 3 The effect of host-derived RNA interference (RNAi) and ectopic expression of M. incognita MiPDI1 in Arabidopsis on RKN infection. (a) MiPDI1 expression in three independent, homozygous pdi-Ri lines, two gfp-RNAi lines and the wild type (WT) were determined 10 dpi by RT-qPCR. The data shown are means ±SE from three independent biological replicates. (b) Phenotypes of nematodes in different Arabidopsis line roots. Acid fuchsin was used to stain Arabidopsis roots after M. incognita infection 35 days. For each line, at least 10 roots were observed, and the experiment was repeated three times. Bars represent 300 μm. (c) In vivo RNAi of MiPDI1 in Arabidopsis reduced the level of M. incognita infection. Mean numbers of galls and nematodes (parasitic juveniles at any stage and females) were determined at 35 dpi in various Arabidopsis lines. Data are presented as means ±SD (n≥30). Similar results were obtained in three independent experiments. One representative experiment is shown. (d) MiPDI1 expression led to a reproducible increase in Arabidopsis susceptibility to M. incognita. Total numbers of egg masses in two independent MiPDI1 transgenic lines were counted at 35 dpi. Two independent experiments were conducted for each line, and 30 plants were analysed per line. (a, c, d) Different letters indicate statistically significant difference in two-way ANOVA with Tukey's multiple comparisons test ($P<0.05$).

80x106mm (300 x 300 DPI)

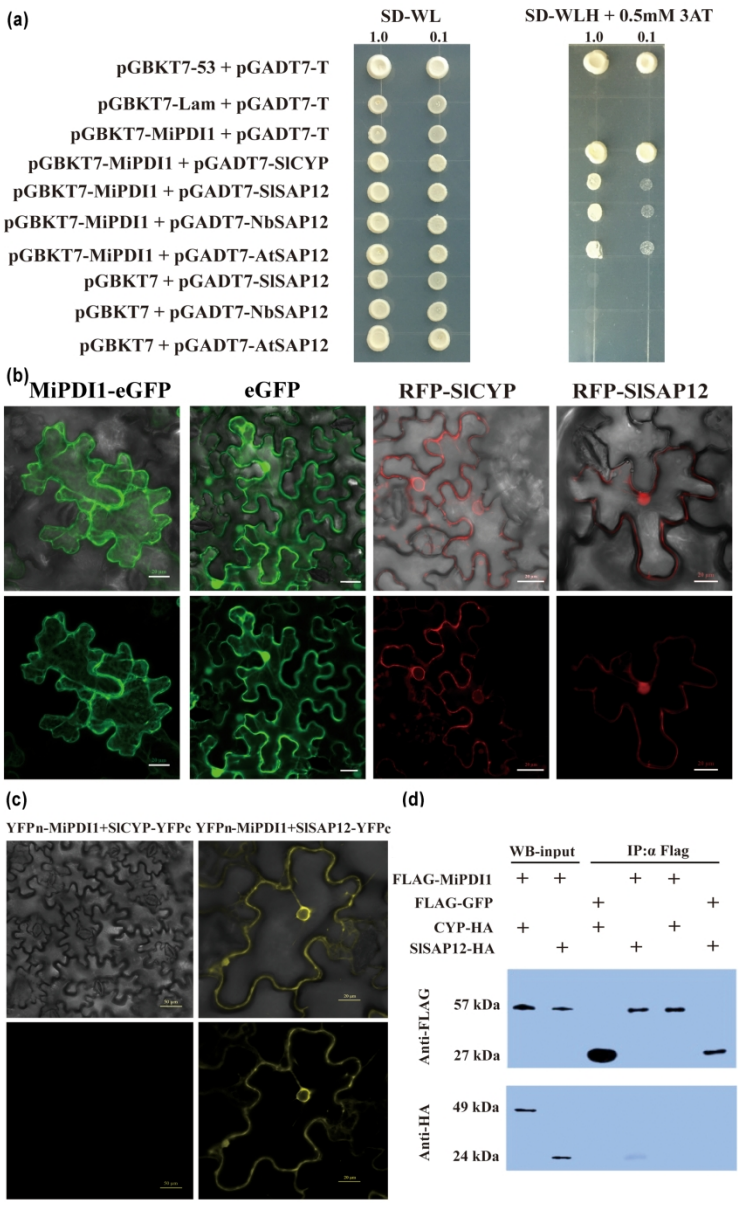

Fig. 4 MiPDI1 interacts with Arabidopsis and Solanaceae stress-associated proteins SAP12. (a) Pairwise yeast two-hybrid tests were performed to investigate the interactions between MiPDI1 and cysteine proteinase (SlCYP) or SAP12 proteins from S. lycopersicum (SlSAP12), N. benthamiana (NbSAP12) and A. thaliana (AtSAP12). Left column, yeast cell growth carrying the baits (in pGBKT7 vector) and preys (in pGADT7) grown on SD/-trp-leu medium indicating successful transformation of the yeast with both plasmids; right column, yeast cell growth on the selective triple dropout medium (SD/-trp-leu-his) following the addition of 3-amino-1,2,4-triazole (3AT) indicating protein interaction. Yeast cells containing p53 and SV40 were used as positive control. (b) Subcellular localisation of MiPDI1, GFP-SlCYP and SlSAP12 in N. benthamiana. MiPDI1-eGFP, eGFP, SlCYP-RFP and SlSAP12-RFP were transiently expressed in N. benthamiana leaves. Signals were detected 48 h after infiltration. Images were captured by confocal microscopy (Zeiss LSM 880, Germany). Scale bar, 20 μm. (c) Bimolecular fluorescence complementation (BiFC) visualisation of the interaction between MiPDI1 and SlSAP12. N. benthamiana leaves were transformed with YFPn-MiPDI1 and SlSAP12-YFPc or SlCYP-YFPc. Images were obtained 36 h after co-expression. Signals were observed in the cytoplasm in leaves co-infiltrated with YFPn-MiPDI1 and SlSAP12-

YFPc. (b, c) At least ten cells from three leaves of three different plants were observed with similar results. YFP, yellow fluorescent protein. Scale bar, 20 μm or 50 μm. (d) Co-immunoprecipitation (Co-IP) analysis of MiPDI1 interacting with SlSAP12. FLAG-MiPDI1 or FLAG-GFP was transiently co-expressed with SlSAP12-HA or SlCYP-HA in tobacco leaves. Co-IP was performed with anti-FLAG M2 affinity gel resin (Sigma-Aldrich), and the isolated protein was detected by western blotting with an anti-FLAG antibody to detect MiPDI1 or eGFP, and an anti-HA antibody to detect SlSAP12 or SlCYP. eGFP, enhanced green fluorescent protein.

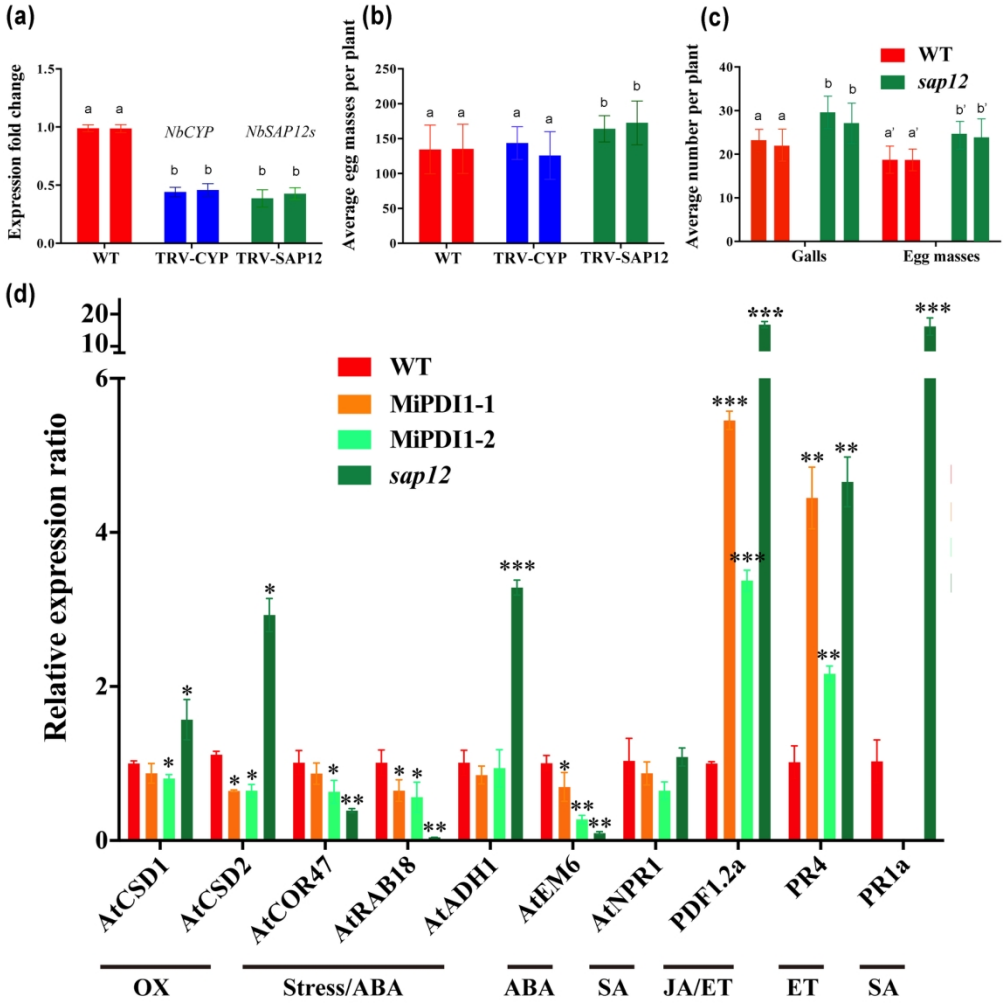

Fig. 5 Effect on susceptibility to M. incognita of virus-induced gene silencing (VIGS) of NbSAP12s and NbCYP in N. benthamiana, and of the A. thaliana sap12 knockout mutant. (a) Levels of NbSAP12s and NbCYP transcripts in N. benthamiana following silencing, as assessed by real-time quantitative PCR (RT-qPCR). Error bars represent the standard errors for 10 biological replicates, and the results of two independent experiments were presented. (b) N. benthamiana plants in which NbSAP12s was silenced were more susceptible to M. incognita, whereas those in which NbCYP was silenced were not significantly different from the wild type in terms of susceptibility, as indicated by the mean numbers of egg masses on plant roots. Error bars represent the mean ± SD (n≥15). All experiments were performed twice, and at least 15 plants were analysed per treatment. (c) The sap12 mutant line (SALK_014706) was more susceptible to M. incognita, as shown by the mean numbers of egg masses and galls in roots. Error bars represent the mean ± SD (n≥20). Two independent experiments were conducted and yielded similar results, with at least 30 plants analysed per treatment. (a, b, c) Different letters indicate statistically significant difference in two-way ANOVA with Tukey's multiple comparisons test ($P < 0.05$). (d) Levels of expression for stress- and defence-related genes in MiPDI1-expressing lines (MiPDI1-1 and MiPDI1-2), the sap12 mutant line (SALK_014706) and the wild type (WT). The genes considered were AtCSD1 (cytosolic Cu/Zn superoxide dismutase), AtCSD2 (chloroplastic Cu/Zn superoxide dismutase), AtCOR47 and AtRAB18 (from the dehydrin protein family), AtADH1 (catalysing the reduction of acetaldehyde with NADH as reductant), AtEM6 (stress-induced protein), AtNPR1 and AtPR1a (SA-mediated defence response marker gene), AtPDF1.2a (encoding ethylene- and jasmonate-responsive plant defences), AtPR4 (ethylene-responsive pathogenesis-related protein). AtOXA1 (AT5G62050) and AtUBP22 (AT5G10790) were used as internal controls. Expression levels were measured by real-time quantitative PCR (RT-qPCR) and the data shown are means ±SD (n = 4).

Asterisks indicate significant differences for single stress- and defence-related gene among different plant lines by one-way ANOVA with Dunnett's multiple comparisons test (*P < 0.05, ** P<0.01, *** P <0.001).

160x160mm (300 x 300 DPI)